Articles

Slow Conformational Dynamics in the Hamster Prion Protein†

Kazuo Kuwata,*,# Yuji O. Kamatari,⊥ Kazuyuki Akasaka,‡ and Thomas L. James*,§

Department of Biochemistry and Biophysics, School of Medicine, Gifu University, Gifu 500-8705 Japan, Cellular Signaling Laboratory, RIKEN Harima Institute, Hyogo, 679-5148 Japan, Department of Biotechnological Sciences, School of Biology-Oriented Science and Technology, Kinki University, Wakayama, 649-6493 Japan, and Department of Pharmaceutical Chemistry, 600 16th Street, Genentech Hall, University of California, San Francisco, California, 94143-2280 USA

Received November 25, 2003; Revised Manuscript Received February 9, 2004

ABSTRACT: Although the mechanism of the conformational conversion from the cellular (PrP^C) to the scrapie (PrP^{Sc}) form of animal prion proteins has yet to be elucidated, evidence is accumulating that may provide insight into the conversion process at atomic resolution. Here we show critical aspects of the slow fluctuation dynamics of the recombinant hamster prion protein, rPrP(90−231), based on NMR relaxation analysis using Carr-Purcell-Meiboom-Gill (CPMG) experiments, and compare them in detail with results from high-pressure NMR. Residues exhibiting slow fluctuations on the time scale of microseconds to milliseconds are mainly localized on helices B and C (172−193 and 200−227), which include locally disordered regions in an intermediate conformer, PrP*, identified previously by high-pressure NMR [Kuwata, K., et al., (2002) *Biochemistry* 41, 12277−12283]. Moreover, chemical shift differences between two putative exchanging conformers obtained by the CPMG relaxation analysis and the linear component of the pressure-induced chemical shift changes are reasonably correlated at individual residue sites. These observations suggest that both the CMPG relaxation and the pressure shifts reflect slow conformational fluctuations and that these slow motions in PrP^C are related to the trajectories leading to the transition to PrP*.

Prions cause neurodegenerative diseases, such as scrapie in sheep, bovine spongiformencephalopathy (BSE) in cattle, Creutzfeldt-Jakob disease (CJD), Gerstmann-Sträussler-Scheinker syndrome (GSS), fatal familial insomnia (FFI), kuru, and a new variant of CJD in humans (*1*−*3*). These diseases are associated with conversion of the normal cellular form of the prion protein (PrP^C) to a pathogenic scrapie form (PrP^{Sc}), which is apparently the infectious agent in transmitted forms of the disease (*3*, *4*). The sequences of PrP^{Sc} and the noninfectious precursor PrP^C are identical (*5*). Although both isoforms are chemically identical, they possess very different physicochemical properties. PrP^C is substantially helical, but PrP^{Sc} has ~40% β-sheet (*6*).

The three-dimensional structure of PrP^C was first elucidated for the mouse, Mo PrP (121−231) (*7*), and the hamster species, SHa PrP (90−231) (*8*), by NMR. Subsequently, structures for bovine (*9*) and human (*10*) species were elucidated. While there are some species-specific differences, the structures are similar in that residues 128−231 constitute a globular fold with three α-helices, a small, imperfectly formed and conformationally flexible β-sheet composed of antiparallel strands S1 and S2, an N-terminal segment up to residue 113 completely disordered and, at least in the hamster species, a hydrophobic cluster (residues 113−128) with multiple interconverting conformers (*11*).

NMR studies of dynamics in the PrP^C structure were reported (*11*, *12*) using heteronuclear NOE, T_1, T_2, and off-resonance $T_{1\rho}$ relaxation time measurements (*12*). The results are consistent with the static picture of PrP^C, i.e., the central portions of helices B and C form a relatively rigid core, but the remainder of the globular domain and helix A are more flexible on a picosecond-to-nanosecond time scale. Slow conformational fluctuations on the microsecond-to-millisecond time scale were observed only for the small β-sheet and the hydrophobic cluster (*11*, *12*).

However, our recent results for conformational fluctuations by high-pressure NMR were quite different from that static picture, possibly due to the difference in the time scale of the fluctuations (*13*). Consequently, here we examined NMR relaxation results for SHa PrP (90−231) using the Carr-Purcell-Meiboom-Gill (CPMG) method (*14*) as well as standard T_1, T_2, and NOE measurements, together with a

† Supported in part by Grants-in-Aid for Scientific Research from the Ministry of Education, Culture, Sports, Science and Technology of Japan (14380314, 14037224) and by the Gifu Prefecture Brain Research Foundation.

* To whom correspondence should be addressed. E-mail: james@picasso.ucsf.edu; tel.: (415) 476-1916; fax: (415) 502-8298 or e-mail: kuwata@cc.gifu-u.ac.jp; tel: +81-582-67-2227; fax: +81-582-67-2962.

Gifu University.

⊥ RIKEN Harima Institute.

‡ Kinki University.

§ University of California.

10.1021/bi036123o CCC: $27.50
Published on Web 03/26/2004

further detailed analysis of the high-pressure NMR results. All of these data pertaining to prion protein dynamics are examined in the context of biological and clinical observations (*15*).

MATERIALS AND METHODS

Samples. Expression, isotopic labeling, purification, and considerations for proper refolding of recombinant Syrian hamster prion protein rPrP (90−231) have been described previously (*11*, *13*). Purified rPrP (90−231), labeled uniformly with ^{15}N, was lyophilized before refolding. Samples were analyzed by mass spectroscopy, circular dichroism, and Fourier transform infrared spectroscopy to ensure the refolded rPrP (90−231) resembles PrP^C, i.e., is largely α-helical.

NMR Measurements. The online high-pressure NMR system contains the protein solution in a quartz tube cell that endures pressures of ≥2500 bar. The cell was connected to a high-pressure line via frictionless Teflon pistons that separate the protein solution from the pressure mediator (kerosene) in a separator cylinder (BeCu). The cell body (inner diameter 1 mm, outer diameter 3 mm) is positioned in a commercial 5-mm NMR probe (Bruker). Pressure was regulated to a desired value between 1 and 2500 bar with a remote hand-pump and maintained at that value during signal accumulation. For 1D and 2D NMR measurements, samples were dissolved in 95% ^1H_2O/5% ^2H_2O containing 20 mM sodium acetate, pH 5.2, to make a 1 mM protein solution. As chemical shift references, trace amounts of sodium 3-trimethylsilyl-(2,2,3,3-^2H)-tetradeuteriopropionate (TSP-d_4) and dioxane were added to the solution. The dioxane resonance remains unchanged with pressure (3.750 ppm from TSP at 1 bar). Relaxation time measurements were performed in standard Shigemi tubes with 11.7 T (Varian Inova 500) and 18.8 T NMR spectrometers (Bruker Avance 800).

Reduced Spectral Density Mapping. ^{15}N longitudinal (T_1) and transverse (T_2) relaxation times and {^1H}-^{15}N heteronuclear NOEs were measured using two different magnetic fields, 11.7 T (500 MHz proton frequency) and 18.8 T (800 MHz). Several peaks are overlapped and are not presented here. For residues 100−231, the R_1 (=$1/T_1$) rates are relatively invariant around 1.5 s^{-1} at 11.7 T. At 18.8 T, for residues 128−231, they are all approximately 1.0 s^{-1}. For residues 100−110, R_1 values are about 1.5 s^{-1}, indicating the relative invariance to the magnetic field strength, which is commonly observed for natively unfolded protein (*16*, *17*). The reduced spectral density function, $J(\omega)$, provides insights into the motion of the N−H bond vector at five frequencies: 0, ω_{N1} (0.32 gigaradian (grad)/s), ω_{N2} (0.51 grad/s), $0.87\omega_{H1}$ (2.73 grad/s), and $0.87\omega_{H2}$ (4.37 grad/s), where 1 and 2 denote angular velocities at 11.7 and 18.8 T, respectively. The largest value of $J(0)$ is ~6 ns at 11.7 T and ~5 ns at 18.8 T. The different $J(0)$ values at 11.7 and 18.8 T demonstrate the inherent limitation of deriving absolute $J(0)$ values from first-order reduced spectral density mapping. The $J(0)$ values at 11.8 T are used in Figure 6a (vide infra).

Slow Fluctuation Analysis. Values of the exchange lifetime τ_{ex} were calculated from the dependence of the signal intensities on interpulse spacing in the CPMG experiment (*13*, *14*). The pulse sequence for measuring the ^{15}N R_2 values (*18*−*20*) was used with modifications for averaging in-phase and antiphase coherence (*21*, *22*).

The apparent transverse relaxation rate with two-site chemical exchange can be expressed as (*14*)

$$R_2^* = R_2 + \tau_{ex} f_1 f_2 (\Delta\omega)^2 \left[1 - \frac{2\tau_{ex}}{\tau_{cp}} \tanh\left(\frac{\tau_{cp}}{2\tau_{ex}}\right)\right] \quad (1)$$

where τ_{cp} is the delay between 180° pulses in the CPMG sequence, and $\Delta\omega$ is the difference in chemical shift of the nucleus in the two conformational states. τ_{ex} (= $\tau_{-1}f_1 = \tau_1 f_2$) is the exchange time constant. f_1 and f_2 (= $1 - f_1$) are the fractions of populations of the two conformational states, and τ_1 and τ_{-1} are forward and the reverse exchange time constants, respectively. R_2 is the pure transverse relaxation rate due to the molecular motion on the time scale of picoseconds to nanoseconds without the slow exchange contribution on the microsecond-to-millisecond time scale. Numerical calculation using the exact equation (*23*) shows that eq 1 is accurate within 5% when $\Delta\omega < 4$ ppm and $\tau_{cp}/\tau_{ex} < 10^{-2}$. In our case, $(f_1 f_2)^{1/2}\Delta\omega \sim 0.1$ kHz, and $\tau_{ex} \sim 0.002$ s. However, since the exact equation is still a monotonic function of $\Delta\omega$ and τ_{ex}, we may be able to characterize these parameters qualitatively rather than quantitatively, even when $(f_1 f_2)^{1/2}\Delta\omega > 0.1$ kHz, and $\tau_{ex} > 0.002$ s. This is illustrated by representative examples of nonlinear fits that are shown in Supporting Information.

High-Pressure NMR Analysis. In general, the conformation of a protein molecule in solution may consist of an equilibrium mixture of conformers differing in topology of folding (e.g., between the native conformer N and an intermediate partially folded conformer I), in partial molar volume V, as well as in thermodynamic stability ΔG. In this situation, the equilibrium constant K between N and I may change with pressure according to the relation:

$$K = [I]/[N] = \exp(-\Delta G/RT) \quad (2)$$

where

$$\Delta G = G(I) - G(N) = \Delta G_0 + \Delta V(p - p_0) - (1/2)\Delta\beta V (p - p_0)^2 \quad (3)$$

ΔG and ΔG_0 are the Gibbs free energy changes from N to I at pressure p and p_0 (= 1 bar), respectively, ΔV is the partial molar volume change, $\Delta\beta$ is the change in compressibility coefficient, R is the gas constant, and T is the absolute temperature (*13*).

The pressure dependence of the chemical shifts was analyzed according to

$$\delta_i = a_i + b_i p + c_i p^2 \quad (4)$$

where δ_i is the chemical shift for the ith residue, and a_i, b_i, and c_i are independent linear and nonlinear coefficients of the pressure-induced shift, respectively.

Curve fitting was performed using SigmaPlot2001 (SPSS Science, Chicago, IL) on all observed data.

RESULTS

Spectral Densities. First, we measured the reduced spectral density function (*18*), $J(\omega)$, for almost all residues of PrP^C, which would provide insights into the motion of the N−H bond vector at five frequencies 0, 0.32, 0.51, 2.73, and 4.37

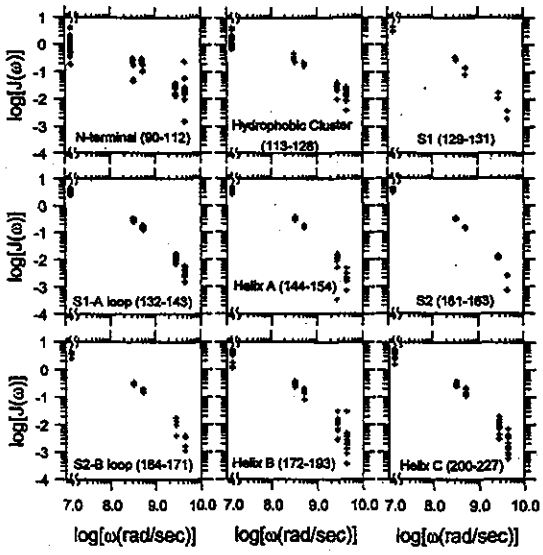

FIGURE 1: The reduced spectral density function, $J(\omega)$, of the N−H bond vector is shown for different regions of PrP^C at five frequencies: 0, ω_{N1} (0.32 grad/s), ω_{N2} (0.51 grad/s), $0.87\omega_{H1}$ (2.73 grad/s), and $0.87\omega_{H2}$ (4.37 grad/s), where subscripts 1 and 2 denote angular velocities at 11.7 and 18.8 T, respectively.

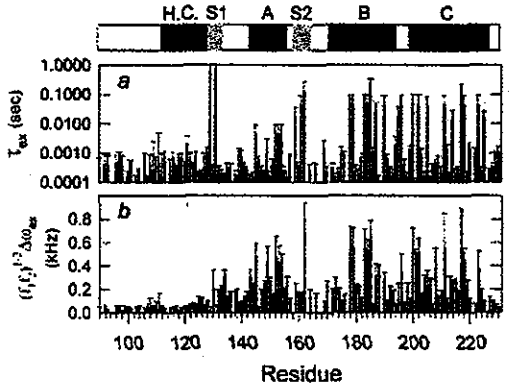

FIGURE 2: (a) Slow exchange lifetimes (τ_{ex}) obtained using the CPMG dispersion method (*14*) plotted as a function of residue number. (b) $\{f_1f_2\}^{1/2}\Delta\omega_{ex}$ plotted as a function of residue number. $\Delta\omega_{ex}$ is the difference in chemical shift of the nucleus in the two conformational states. f_1 and f_2 (= $(1 - f_1)$) are the populations of the two conformational states.

gigaradian (grad)/s using two static magnetic field strengths, 11.7 and 18.8 T. As shown in Figure 1, $J(0)$ values for the N-terminal and hydrophobic cluster are relatively low and rather dispersed, while those for residues in S1 and S2 β-strands and helices B and C are comparatively high. Large $J(0)$ values reflect the global tumbling motion (*12*). We note that J (4.37 grad/s) values are also quite heterogeneous for N-terminal regions and helices B and C, suggesting a large degree of flexibility.

Slow Exchange Dynamics. We obtained evidence of slow conformational exchange from the τ_{cp} dependence of the CPMG dispersion experiments. By assuming two-site exchange, we apply eq 1 (see Materials and Methods) to the CPMG relaxation dispersion data. Figure 2a shows lifetimes corresponding to the slow exchange rates obtained (*14*). Values for the slow exchange time constant, τ_{ex}, and the

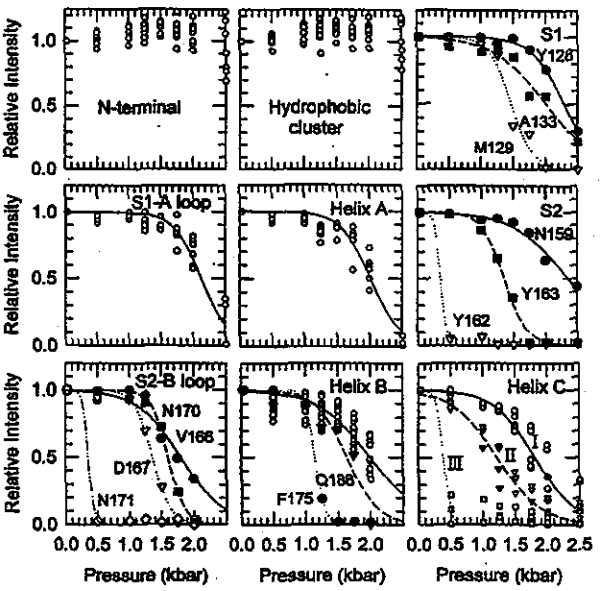

FIGURE 3: Integrated intensities of amide resonances in HSQC spectra as a function of pressure. The transition profiles are divided into nine groups according to secondary structure elements of PrP^C. The multiple values at each pressure correspond to different residues within a structural region. Lines are from curve fitting using eq 2. The transition from the native conformation varies from site to site, showing that the pressure stability of rPrP(90−231) is site-dependent.

difference in chemical shifts ($\Delta\omega$), shown in Figure 2b, were calculated using eq 1. The τ_{ex} values are on the microsecond-to-millisecond time scale, and the relatively large $\Delta\omega$ values are mainly found in the β-strands S1 and S2 and helices B and C. Specifically, residues with τ_{ex} larger than 0.01 s are M129, G131, N159, V161, Y162, D178, C179, T183, I184, L185, H187, T190, G195, E196, E200, D202, I205, E211, C214, Q217, Y218, Q223, and Y225. They are mapped by yellow in Figure 4a.

High-Pressure NMR. Under high pressure, the population of the native state is generally decreased and, if present at all, that of an intermediate state is increased, because the partial molar volume of the native structure is generally larger than that of the intermediate structure, since it is presumably less tightly folded. Pressure-induced conformational transitions are generally less cooperative than those of other perturbations, such as temperature or denaturant concentration, because, in the native conformation, each affected residue is adjacent to a cavity with specific volume. Therefore, pressure-induced disorder of the native conformation often varies from site to site, showing that the thermodynamic stability of rPrP(90−231) is site dependent. We categorized the behaviors of the integrated intensities of amide residues in HSQC spectra as a function of pressure into nine groups according to secondary structure elements of the protein, as shown in Figure 3. Lines are theoretically generated by fitting eq 2, in Materials and Methods, to the experimental data points. Cross-peak intensities from the N-terminus and the hydrophobic cluster were essentially invariant with pressure, while intensities for residues 128−231 dramatically decreased with pressure, almost disappearing by 2500 bar. This indicates that the major conformational changes are occurring. The relative inertness of spectral

features to pressure is a general property of a disordered conformer. There is substantial heterogeneity in pressure stability among the secondary structure elements. The S1-A loop and helix A were most stable with pressure change, and their transitions occurred uniformly over their constituent residues. Pressure-induced transitions of helix B residues also occurred rather uniformly, with the exception of F175 and Q186. The pressure stability is determined mainly by two factors, the stability at 1 bar (ΔG_0) and ΔV, neglecting the $\Delta\beta$ contribution (eq 3). By extrapolating eq 3 to 1 bar and neglecting data for F175 and Q186, we obtain average thermodynamic stabilities ΔG_0 of helix A and helix B at 1 bar to be 5.2 and 3.0 kcal/mol, respectively. The results clearly indicate that helix B has much less stability than helix A. Other secondary structure elements were even less stable against pressure, and their transitions were more heterogeneous. Transitions of residues in β-strands S1 and S2, the S2-B loop and helix C occurred quite heterogeneously at pressures between 500 and 2500 bar. Transitions were most varied for helix C. They are roughly categorized into three groups (see Figure 3); group I (○: composed of most residues), group II (▽; V210, M213, Q217, K220), and group III (□; K204, I205, Q219).

Thermodynamic analysis, extrapolated to 1 bar via eq 2, gave ΔG_0 values of 3.4 kcal/mol for group I and 2.1 kcal/mol for group II. The group II residues are located essentially at the interface with β-strands S1 and S2, suggesting that the apparent low stability arises from increased conformational disorder of these residues relative to strands S1 and S2. K204, I205, Q219 in group III of helix C, Y162 of S2, N171 of the S2-B loop and F175 of helix B were exceptionally unstable and underwent transitions below 1000 bar. Residues M129, Y163, D167, N170, F175, V210, M213, Q217, and K220 exhibited moderate instability and undergo transitions around 1500 bar. They are mapped in magenta and yellow, respectively, on the NMR structure (*11*) in Figure 4b. Although residues with pressure-induced instability are distributed mainly around the interface between S2 and helix C as shown in Figure 4b, those with any significant slow fluctuations with τ_{ex} more than 0.01 s are distributed more widely and cover S1, S2, helices B and C, as shown in Figure 4a.

Correlation between Fluctuation-Induced and Pressure-Induced Chemical Shift Changes. We have compared the fluctuation- and pressure-induced chemical shift changes, since the measurements are not a priori related. Figure 5a is the plot of the chemical shift changes of amide ^{15}N nuclei induced by fluctuation, $\{f_1f_2\}^{1/2}\Delta\omega_{ex}$, with τ_{ex} larger than 1 ms, against the linear components of the pressure dependence of the ^{15}N chemical shifts (*13*). Although the amplitudes of the former are about 10 times larger than the latter, they are reasonably well correlated. On the other hand, there is no evident correlation between the chemical shift changes of amide ^{15}N nuclei induced by slow exchange fluctuations, $\{f_1f_2\}^{1/2}\Delta\omega_{ex}$ with τ_{ex} larger than 1 ms, and any (total or nonlinear) component of the pressure dependence of the ^{15}N chemical shifts (data not shown). Correlations between the chemical shift changes of amide ^{15}N nuclei induced by fluctuation, $\{f_1f_2\}^{1/2}\Delta\omega_{ex}$ with τ_{ex} on the time scale of microsecond and any pressure dependence of the ^{15}N chemical shifts are not evident.

DISCUSSION

Dynamic Features of the Natively Unfolded N-Terminal Region. Since regions in the hydrophobic cluster (113−128) are only transiently folded (*11*), no significant slow dynamics nor any significant conformational transition was observed (Figures 1−3). However, the hydrophobic cluster is apparently necessary for PrP to convert into PrP^{Sc}. For example, transgenic mice with removal of N-terminal residues beyond residue 93 did not support PrP^{Sc} formation. Interestingly, Tg mice expressing PrP(121−231) develop a cerebellar disorder in the neonatal period implying that much, if not all, of the N-terminal moiety of PrP is necessary for normal function (*24*). Deletion of the C-terminal helices also causes a heritable disorder with severe nerve cell loss (*25*). Therefore, we may assume that the hydrophobic cluster functionally lies within the "death domain", which spontaneously forms the killer conformation via intermolecular interactions such as other conformational diseases (*26*), on the condition that this region is accessible to other pertinent molecules.

Hydrogen bonds apparently exist between M129 and Y163 in the small, unstable β-sheet (*11*), so it is not surprising to see in Figure 3 that M129 and Y163 together exhibit a pressure-induced change. The polymorphism of residue 129, being a valine in many humans, results in different disease phenotypes expressed by the D178N mutation shown in Figure 6f, which can be understood in terms of the structure (*11*). Different clinical manifestations and different prion diseases may result from different conformations of PrP^{Sc} being present. The pressure study further indicates that the region of the S1 strand with methionine at residue 129 is inherently unstable. Residue 129 is near D178, with some evidence that the D178 carboxylate is hydrogen bonded to the Y128 ring hydroxyl (*11*), so conformational fluctuations in helix B can propagate into the S1 strand and proximal hydrophobic cluster. Some amides in the ill-formed β-sheet undergo very slow fluctuations (Figures 2 and 6a,b) and are also affected more readily by pressure (Figures 3 and 6c). That is not surprising, as multiple NMR signals were observed for some β-strand residues (*11*). Both observations emphasize that the β-sheet in PrP^{C} is not very stable. Conceivably, the pressure instability of F175 in helix B is also related to comparatively low stability of S2 and S2-B loop.

Slow Dynamics and Stability of the C-Terminal Helical Region. PrP* was first observed as a metastable intermediate during the unfolding process of SHa rPrP(90−231) with guanidinium chloride (*27*). Other observations have supported the existence of intermediate forms of prions (*28*, *29*). Recently, we characterized some structural features of PrP* (*13*). A small amount of PrP* coexists with native PrP^{C} under nearly physiological conditions (pH 5.2, 30 °C, 1 bar) with the pressure-dependence studies, suggesting that PrP* has disordered B and C helices, while helix A is largely intact (*13*). From the pressure dependence of the signal intensities of individual residues for PrP^{C}, the stability difference of $\Delta G_0 = 2.1$ kcal/mol was obtained for group II residues. This indicates that as much as 1−3% of PrP exists as PrP* at ambient temperature and pressure. Assuming that the signals observed are all from PrP^{C}, the present relaxation analysis indicates that PrP^{C} undergoes millisecond fluctuations particularly in the vicinity of helices B and C.

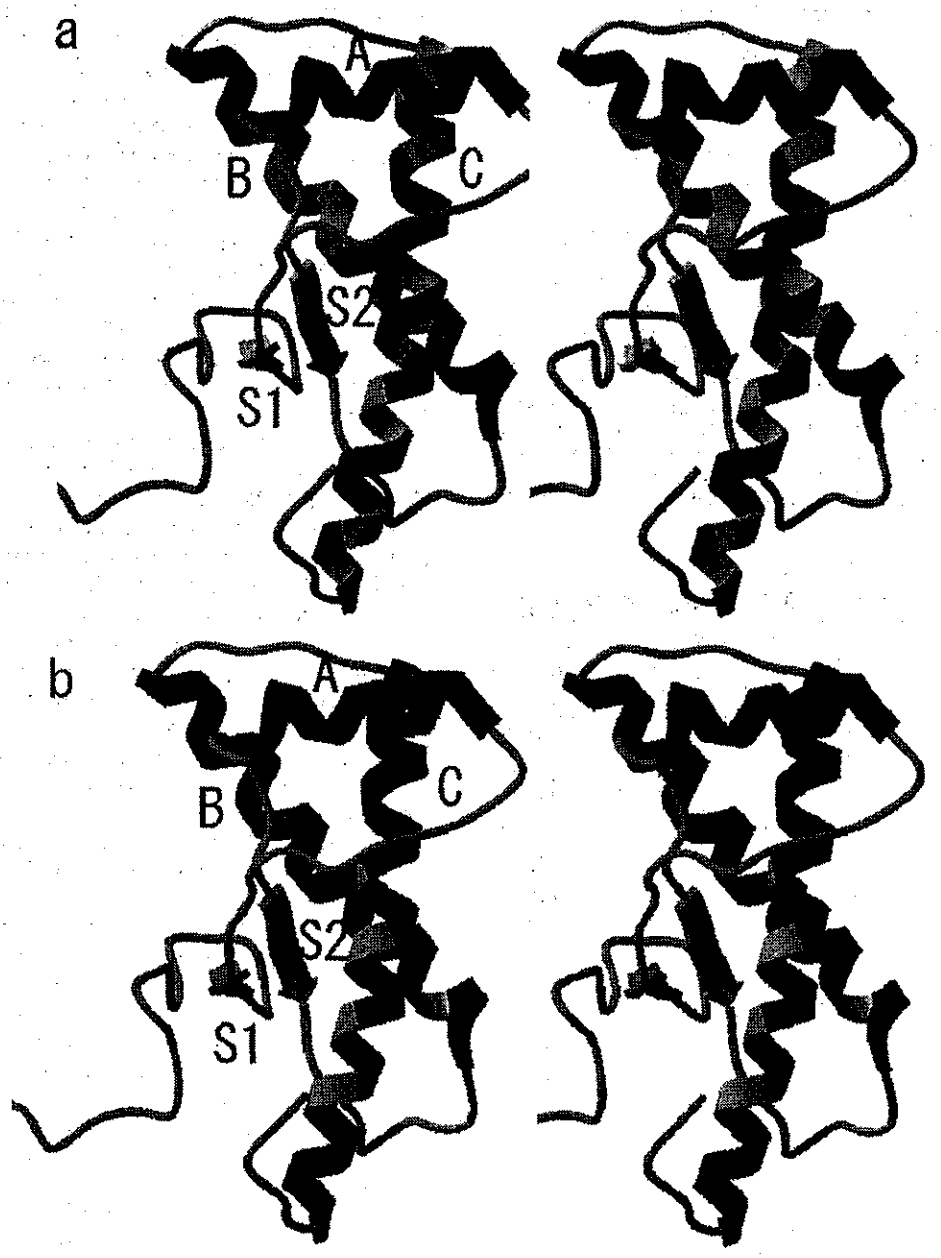

FIGURE 4: In the context of the PrP(90−231) structure, comparison of CPMG T_2 conformational dynamics and high-pressure-induced conformational changes. (a) Residues with τ_{ex} larger than 0.01 s are M129, G131, N159, V161, Y162, D178, C179, T183, I184, L185, H187, T190, G195, E196, E200, D202, I205, E211, C214, Q217, Y218, Q223, Y225, and are mapped in yellow on the NMR structure (*11*). Red represents the helical region, and blue represents other regions. (b) Exceptionally unstable residues that undergo transitions below 1000 bar (K204, I205, Q219 in group III of helix C, Y162 of S2, N171 of the S2-B loop and F175 of helix B), and moderately unstable residues that undergo transitions around 1500 bar (M129, Y163, D167, N170, F175, V210, M213, Q217, and K220) are mapped in magenta and yellow, respectively, on the NMR structure (*11*).

The unstable residues of helices B and C are near a cluster of cavities (*13*), suggesting that the slow dynamics and selective disorder of helices B and C may be related to instability of these cavities. In particular, the HSQC cross-peak intensity reduction observed at relatively low pressures (<500 bar) for group III residue Q219 on helix C is remarkable. As noted previously (*11*), the hamster species, SHa PrP(90−231), and the mouse species, Mo PrP(121−231), differ in that the latter exhibits a break in the helix at Q219. Also, the S2-B loop in SHa PrP (90−231) is well-defined by NMR data but is disordered in Mo PrP (121−231). It should be also noted that Q219 corresponds to the region exhibiting the dominant negative inhibition of prion replication (*26*) (Figure 6d) and also belongs to the protein X binding epitope (*30*) (Figure 6e). Four residues, Q168 in the S2-B loop, Q172 at the beginning of helix B, and T215 and Q219 on helix C, form an epitope that interacts with the putative protein X (*30*), which may well be something other than a protein. Q168, as part of the helical turn, is not in close proximity to the other three residues (Figure 6e).

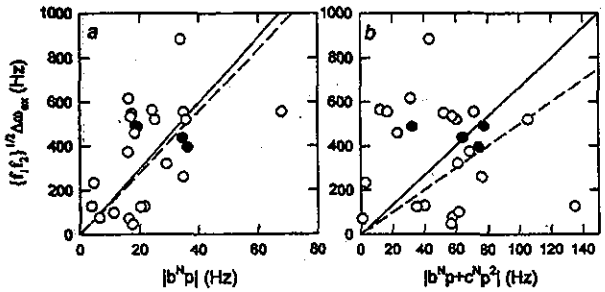

FIGURE 5: Plots of the chemical shift changes of amide ^{15}N nuclei induced by slow fluctuations versus pressure dependencies of the amide ^{15}N chemical shift (*13*). Symbols (○) and (●) indicate residues in helices and in β-sheets, respectively, and lines represent the result of regression analyses. (a) Plot of $\{f_1f_2\}^{1/2}\Delta\omega_{ex}$ for residues with τ_{ex} larger than 1 ms against the linear component of the pressure-dependent chemical shift change of amide ^{15}N resonances. (b) Plot of $\{f_1f_2\}^{1/2}\Delta\omega_{ex}$ for residues with τ_{ex} larger than 1 ms against the total pressure-dependent chemical shift change of amide ^{15}N resonances.

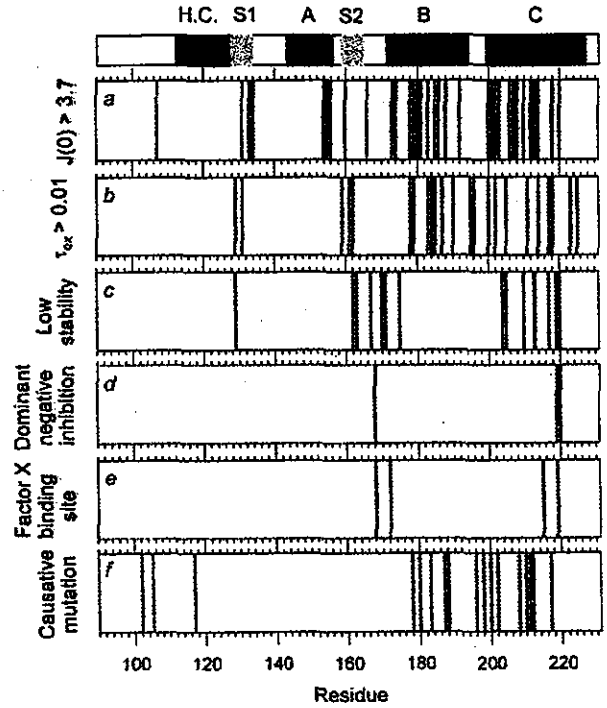

FIGURE 6: Plot of residues whose (a) $J(0)$ values are larger than 3.7 ns, obtained via reduced spectral density mapping, and (b) τ_{ex} values are larger than 0.01 s, obtained using the CPMG method. (c) Residues with low stability detected by high-pressure NMR. (d) Residues with polymorphisms exhibiting dominant negative inhibition of prion replication (*26*). (e) Residues mapped as the protein X binding epitope (*30*). (f) Residues whose mutations cause neurodegenerative diseases in humans.

We can speculate that conformational flexibility in the region facilitates factor X binding.

In PrP^C, slow fluctuations are evidently not connected to observed fast (picosecond-to-nanosecond) fluctuations. Amino acid residues predominantly fluctuating on the millisecond time scale mainly exist in helices B and C, which are also locally disordered in the PrP* intermediate state (*13*). This coincidence suggests that the slow dynamics of the prion protein includes trajectories from the native state to the thermodynamically distinct substate, PrP*. The thermodynamic picture derived from pressure-induced unfolding is not expected from the static NMR structure, nor from the dynamic picture on the picosecond-to-nanosecond time scale, which emphasizes the difference between unstructured N-terminal and structured C-terminal regions (*11*, *12*). Logically, millisecond time scale fluctuations may be qualitatively different from picosecond-to-nanosecond time scale motions (*31*−*33*). The overall coincidence between the stability and the slow dynamics suggests that the slow fluctuations of PrP occur along the reaction surface of the protein folding (*32*). However, the fast motions may just entail low energy fluctuations of the native structure. The curvature of the reaction surface for protein folding may not necessarily correspond to the local energy surface around the native PrP^C structure.

Correlations between Slow Fluctuations under Physiological Conditions and Pressure-Dependent Conformational Changes. The NMR relaxation analysis gives residue-specific amide chemical shift differences between two putative conformers that are considered to be mutually interconverting. These differences should reflect the amplitude of the conformational fluctuation at individual residue sites. On the other hand, from the relation between volume fluctuation and compressibility, pressure-induced chemical shift changes are also correlated with the amplitude of fluctuation at individual residues. As shown in Figure 5a, the chemical shift changes of amide ^{15}N nuclei induced by fluctuation, $\{f_1f_2\}^{1/2}\Delta\omega_{ex}$ with τ_{ex} larger than 1 ms, are correlated with the linear component of the pressure dependency of the ^{15}N chemical shift (*13*). This may suggest that slow fluctuations at ambient pressure are occurring within the basic folded subensemble (*34*). The basic folded subensemble is the "ensemble" of the native conformations with essentially the same compressibility exhibiting the linear pressure-dependent chemical shift changes. When they exhibit any nonlinear behavior, we presume it to be a transition from the basic folded structure to the low-lying excited state (*35*).

The amplitudes of the chemical shift fluctuations are about 10 times larger than those of the pressure-induced chemical shift changes. The average ^{15}N chemical shift difference between 1 and 2.5 kbar is ~0.1 ppm, which corresponds to a ψ angle of ~0.4° (*36*). On the other hand, the fluctuation of the ψ angle obtained by the CPMG relaxation experiment is ~4°, which is basically consistent with the results of many MD simulations (*37*). The Gibbs free energy of a protein is generally defined as a function of pressure (P) and temperature (T). In a thermal denaturation process under constant pressure, the entropic change ($T\Delta S$) is the main driving force, while in pressure denaturation at constant temperature, the volume change ($-P\Delta V$) is the major driving force. However, under approximately physiological conditions, a fluctuation may occur along a direction between them, as shown in Figure 7. The pressure-induced conformational changes emphasize the intermediate conformers with large ΔV, while temperature-induced conformational changes emphasize those with large ΔS. However, if a protein could fluctuate in a P/T plane freely during fluctuations, a small population may have a chance to reach a conformation with higher energy along the trajectories. This dynamic event may occur rarely, either because of the high energetic barrier (fast motion but with low probability) or by following a winding pathway along the rugged surface (slow motion). Either way, populat-

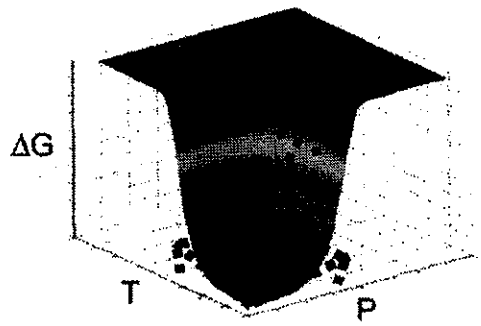

FIGURE 7: A sketch of the free energy landscape of a protein as a function of pressure (P) and temperature (T). Arrows on the right and left indicate the pressure and the temperature dependence, respectively, of the Gibbs free energy within the basic folded subensemble. The central arrow shows the effect of a fluctuation under physiological conditions occurring in a P/V plane.

ing the higher energy state occurs slowly.

Many intermediates in various proteins have been detected using high-pressure NMR (*34*). Why is pressure perturbation so sensitive for detecting intermediates compared to temperature perturbation? One reason may be that many intermediates are better defined in terms of volume than entropy. As long as protein folding occurs hierarchically with distinct volume changes, high-pressure NMR is quite useful to observe it. However, if an intermediate conformation has a volume similar to the native conformation, it may not be detected. Second, it must be noted that oligomers or aggregates, including amyloids, tend to dissociate into monomers under high pressure, while proteins generally tend to aggregate at high temperature. High-pressure NMR may prove advantageous for study of such intermolecular interactions.

CONCLUSIONS

Interaction between the C-terminal helical region and the hydrophobic cluster region of PrP^C was previously observed (*11*, *13*), and both regions are required for the infectivity (*38*). As noted, the pressure-induced collapse of cavities probably accounts for the observed NMR signal changes in helices B and C and in the S2-B loop and the β-strand S2. Because the hydrophobic cluster is also in contact with S2 and helix B (*11*), as shown in Figure 4, conformational transitions in this region can transduce a switch to possibly involve most of the structural elements identified in rPrP-(90−231) in promoting the $PrP^C \rightarrow PrP^{Sc}$ transformation. Pathogenicity itself must be directly related to the intermolecular interaction around the hydrophobic cluster regions, and the C-terminal helices may naturally prevent this intermolecular interaction. Modeling of PrP^{Sc} structure using electron microscopy has yielded models with intramolecular β-sheets while maintaining some helix structure (*39*). While progress on this difficult project is admirable, it is not possible at this stage to know with certainty whether the helices in PrP^{Sc} correspond precisely to those in PrP^C. PrP* presumably corresponds to an intermediate in the conversion process. Therefore, disease-causing mutations can increase the population of PrP*, which enables access to the hydrophobic cluster via the local conformational disorder of helices B and C. This may promote the conformational conversion process by intermolecular interaction at the hydrophobic cluster, resulting in the intermolecular β-sheet formation characteristic of PrP^{Sc}.

SUPPORTING INFORMATION AVAILABLE

Representative examples of the nonlinear curve fits of the relaxation dispersion data. This information is available free of charge via the Internet at http://pubs.acs.org.

REFERENCES

1. Chazot, G., Broussolle, E., Lapras, C. I., Blättler, T., Aguzzi, A., and Kopp, N. (1996) New Variant of Creutzfeldt-Jakob Disease in a 26-Year-Old French Man. *Lancet 347*, 1181.
2. Will, R. G., Ironside, J. W., Zeidler, M., Cousens, S. N., Estibeiro, K., Alperovitch, A., Poser, S., Pocchiari, M., Hofman, A., and Smith, P. G. (1996) A New Variant of Creutzfeldt-Jakob Disease in the UK. *Lancet. 347*, 921−925.
3. Prusiner, S. B. (1982) Novel proteinaceous infectious particles cause scrapie. *Science 216*, 136−144.
4. Prusiner, S. B. (1991) Molecular Biology of Prion Diseases. *Science 252*, 1515−1522.
5. Stahl, N., Baldwin, M. A., Teplow, D. B., Hood, L., Gibson, B. W., Burlingame, A. L., and Prusiner, S. B. (1993) Structural studies of the scrapie prion protein using mass spectrometry and amino acid sequencing. *Biochemistry 32*, 1991−2002.
6. Pan, K.-M., Baldwin, M., Nguyen, J., Gasset, M., Serban, A., Groth, D., Mehlhorn, I., Huang, Z., Fletterick, R. J., Cohen, F. E., and Prusiner, S. B. (1993) Conversion of α-Helices into β-Sheets Features in the Formation of the Scrapie Prion Proteins. *Proc. Natl. Acad. Sci. U.S.A. 90*, 10962−10966.
7. Riek, R., Hornemann, S., Wider, G., Billeter, M., Glockshuber, R., and Wüthrich, K. (1996) NMR Structure of the Mouse Prion Protein Domain PrP(121−231). *Nature 382*, 180−182.
8. James, T. L., Liu, H., Ulyanov, N. B., Farr-Jones, S., Zhang, H., Donne, D. G., Kaneko, K., Groth, D., Mehlhorn, I., Prusiner, S. B., and Cohen, F. E. (1997) Solution structure of a 142-residue recombinant prion protein corresponding to the infectious fragment of the scrapieisoform. *Proc. Natl. Acad. Sci. U.S.A. 94*, 10086−10091.
9. Lopez Garcia, F., Zahn, R., Riek, R., and Wuthrich, K. (2000) NMR structure of the bovine prion protein. *Proc. Natl. Acad. Sci. U.S.A. 97*, 8334−8339.
10. Calzolai, L., Lysek, D. A., Guntert, P., von Schroetter, C., Riek, R., Zahn, R., and Wuthrich, K. (2000) NMR structures of three single-residue variants of the human prion protein. *Proc. Natl. Acad. Sci. U.S.A. 97*, 8340−8345.
11. Liu, H., Farr-Jones, S., Ulyanov, N. B., Llinas, M., Marqusee, S., Groth, D., Cohen, F. E., Prusiner, S. B., and James, T. L. (1999) Solution structure of Syrian hamster prion protein rPrP(90−231). *Biochemistry 38*, 5362−5377.
12. Viles, J. H., Donne, D., Kroon, G., Prusiner, S. B., Cohen, F. E., Dyson, H. J., and Wright, P. E. (2001) Local structural plasticity of the prion protein. Analysis of NMR relaxation dynamics. *Biochemistry 40*, 2743−2753.
13. Kuwata, K., Li, H., Yamada, H., Legname, G., Prusiner, S. B., Akasaka, K., and James, T. L. (2002) Locally disordered conformer of the hamster prion protein: a crucial intermediate to PrP^{Sc}? *Biochemistry 41*, 12277−12283.
14. Luz, Z., and Meiboom, S. (1963) Nuclear Magnetic Resonance Study of the Protolysis of Trimethylammonium Ion in Aqueous Solution − Order of the Reaction with Respect to Solvent. *J. Chem. Phys. 39*, 366.
15. Prusiner, S. B. (1996) Human Prion Diseases and Neurodegeneration. *Curr. Top. Microbiol. Immunol. 207*, 1−17.
16. Buevich, A. V., and Baum, J. (1999) Dynamics of unfolded proteins: incorporation of distributions of correlation times in the model free analysis of NMR relaxation data. *J. Am. Chem. Soc. 121*, 8671−8672.
17. Uversky, V. N. (2002) Natively unfolded proteins: a point where biology waits for physics. *Protein Sci. 11*, 739−756.
18. Farrow, N. A., Zhang, O., Forman-Kay, J. D., and Kay, L. E. (1995) Comparison of the backbone dynamics of a folded and an unfolded SH3 domain existing in equilibrium in aqueous buffer. *Biochemistry 34*, 868−878.

19. Mulder, F. A. A., Spronk, C. A., E. M., Slijper, M., Kaptein, R., and Boelens, R. (1996) Improved HSQC Experiments for the Observation of Exchange Broadened Signals. *J. Biomolec. NMR. 8*, 223−228.
20. van Tilborg, P. J., Mulder, F. A., de Backer, M. M., Nair, M., van Heerde, E. C., Folkers, G., van der Saag, P. T., Karimi-Nejad, Y., Boelens, R., and Kaptein, R. (1999) Millisecond to microsecond time scale dynamics of the retinoid X and retinoic acid receptor DNA-binding domains and dimeric complex formation. *Biochemistry 38*, 1951−1956.
21. Palmer, A. G., III, Skelton, N. J., Chazin, W. J., Wright, P. E., and Rance, M. (1992) Suppression of the effects of cross-correlation between dipolar and anisotropic chemical shift relaxation mechanisms in the measurement of spin spin relaxation rates. *Mol. Phys. 75*, 699−711.
22. Millet, O., Loria, J. P., Kroenke, C. D., Pons, M., and Palmer, A. G., 3rd. (2000) The Static Magnetic Field Dependence of Chemical Exchange Linebroadening Defines the NMR Chemical Shift Time Scale. *J. Am. Chem. Soc. 122*, 2867−2877.
23. Davis, D. G., Perlman, M. E., and London, R. E. (1994) Direct measurements of the dissociation rate constant for inhibitor-enzyme complexes via the T1 rho and T2 (CPMG) methods. *J. Magn. Reson. B. 104*, 266−275.
24. Shmerling, D., Hegyi, I., Fischer, M., Blättler, T., Brandner, S., Götz, J., Rülicke, T., Flechsig, E., Cozzio, A., von Mering, C., Hangartner, C., Aguzzi, A., and Weissmann, W. (1998) Expression of Amino-Terminally Truncated PrP in the Mouse Leading to Ataxia and Specific Cerebellar Lesions. *Cell 93*, 203−214.
25. Muramoto, T., DeArmond, S. J., Scott, M., Telling, G. C., Cohen, F. E., and Prusiner, S. B. (1997) Heritable disorder resembling neuronal storage disease in mice expressing prion protein with deletion of an alpha-helix. *Nat. Med. 3*, 750−755.
26. Perrier, V., Kaneko, K., Safar, J., Vergara, J., Tremblay, P., DeArmond, S. J., Cohen, F. E., Prusiner, S. B., and Wallace, A. C. (2002) Dominant-negative inhibition of prion replication in transgenic mice. *Proc. Natl. Acad. Sci. U.S.A. 99*, 13079−13084.
27. Zhang, H., Stöckel, J., Mehlhorn, I., Groth, D., Baldwin, M. A., Prusiner, S. B., James, T. L., and Cohen, F. E. (1997) Physical Studies of Conformational Plasticity in a Recombinant Prion Protein. *Biochemistry 36*, 3543−3553.
28. Hornemann, S., and Glockshuber, R. (1998) A scrapie-like unfolding intermediate of the prion protein domain PrP(121−231) induced by acidic pH. *Proc. Nat. Acad. Sci. U.S.A. 95*, 6010−6014.
29. Apetri, A. C., and Surewicz, W. K. (2002) Kinetic intermediate in the folding of human prion protein. *J. Biol. Chem. 277*, 44589−44592.
30. Kaneko, K., Zulianello, L., Scott, M., Cooper, C. M., Wallace, A. C., James, T. L., Cohen, F. E., and Prusiner, S. B. (1997) Evidence for protein X binding to a discontinuous epitope on thecellular prion protein during scrapie prion propagation. *Proc. Natl. Acad. Sci. U.S.A. 94*, 10069−10074.
31. Garcia, A. E., and Hummer, G. (1999) Conformational dynamics of cytochrome *c*: correlation to hydrogen exchange. *Proteins 36*, 175−191.
32. Karplus, M. (2000) Aspects of protein reaction dynamics: deviations from simple behavior. *J. Phys. Chem. B. 104*, 11−27.
33. Komatsuzaki, T., and Berry, R. S. (2001) Dynamical hierarchy in transition states: why and how does a system climb over the mountain? *Proc. Natl. Acad. Sci. U.S.A. 98*, 7666−7671.
34. Akasaka, K. (2003) Highly fluctuating protein structures revealed by variable-pressure nuclear magnetic resonance. *Biochemistry 42*, 10875−10885.
35. Akasaka, K., and Li, H. (2001) Low-lying excited states of proteins revealed from nonlinear pressure shifts in ^{1}H and ^{15}N NMR. *Biochemistry 40*, 8665−8671.
36. Akasaka, K., Li, H., Yamada, H., Li, R. H., Thoresen, T., and Woodward, C. K. (1999) Pressure response of protein backbone structure. Pressure-induced amide ^{15}N chemical shifts in BPTI. *Protein Sci. 8*, 1946−1953.
37. Tai, K., Shen, T., Borjesson, U., Philippopoulos, M., and McCammon, J. A. (2001) Analysis of a 10-ns molecular dynamics simulation of mouse acetylcholinesterase. *Biophys. J. 81*, 715−724.
38. Muramoto, T., Scott, M., Cohen, F., and Prusiner, S. B. (1996) Recombinant scrapie-like prion protein of 106 amino acids is soluble. *Proc. Natl. Acad. Sci. U.S.A. 93*, 15457−15462.
39. Wille, H., Michelitsch, M. D., Guenebaut, V., Supattapone, S., Serban, A., Cohen, F. E., Agard, D. A., and Prusiner, S. B. (2002) Structural studies of the scrapie prion protein by electron crystallography. *Proc. Nat. Acad. Sci. U.S.A. 99*, 3563−3568.

BI036123O